PTEP

Prog. Theor. Exp. Phys. **2018**, 043B07 (18 pages)
DOI: 10.1093/ptep/pty041

Topological susceptibility of QCD with dynamical Möbius domain-wall fermions

S. Aoki[1], G. Cossu[2], H. Fukaya[3,*], S. Hashimoto[4,5], and T. Kaneko[4,5]

[1]*Center for Gravitational Physics, Yukawa Institute for Theoretical Physics, Kyoto 606-8502, Japan*
[2]*School of Physics and Astronomy, The University of Edinburgh, Edinburgh EH9 3JZ, UK*
[3]*Department of Physics, Osaka University, Toyonaka 560-0043, Japan*
[4]*KEK Theory Center, High Energy Accelerator Research Organization (KEK), Tsukuba 305-0801, Japan*
[5]*School of High Energy Accelerator Science, The Graduate University for Advanced Studies (Sokendai), Tsukuba 305-0801, Japan*
*E-mail: hfukaya@het.phys.sci.osaka-u.ac.jp

Received December 11, 2017; Revised February 23, 2018; Accepted March 5, 2018; Published April 21, 2018

We compute the topological susceptibility χ_t of lattice QCD with $2+1$ dynamical quark flavors described by the Möbius domain-wall fermion. Violation of chiral symmetry as measured by the residual mass is kept at $\sim$1 MeV or smaller. We measure the fluctuation of the topological charge density in a "slab" sub-volume of the simulated lattice using the method proposed by W. Bietenholz, P. de Forcrand, and U. Gerber, J. High Energy Phys. **12**, 070 (2015) and W. Bietenholz, K. Cichy, P. de Forcrand, A. Dromard, and U. Gerber, PoS LATTICE **2016**, 321 (2016). The quark mass dependence of χ_t is consistent with the prediction of chiral perturbation theory, from which the chiral condensate is extracted as $\Sigma^{\overline{\rm MS}}(2\,{\rm GeV}) = [274(13)(29)\,{\rm MeV}]^3$, where the first error is statistical and the second one is systematic. Combining the results for the pion mass M_π and decay constant F_π, we obtain $\chi_t = 0.229(03)(13) M_\pi^2 F_\pi^2$ at the physical point.

Subject Index B01, B31, B38, B64

1. Introduction

The topological susceptibility χ_t is an interesting quantity that characterizes how many topological excitations are created in the QCD vacuum. Witten [1] and Veneziano [2] estimated χ_t in the large-N_c (number of colors) limit and showed that it is proportional to the square of the η' meson mass. In real QCD with $N_c = 3$ and light dynamical quarks, however, the argument of Witten and Veneziano is no longer valid. It is not the η' meson but the (zero-momentum mode of the) pion that controls the topological susceptibility.

According to the prediction of $SU(2)$ chiral perturbation theory (ChPT) at leading order (LO), χ_t is expected to be proportional to the quark mass m_{ud}, when the up and down quark masses are degenerate. At one-loop, the quark mass dependence is predicted as [3–5]

$$\chi_t = \frac{m_{ud}\Sigma}{2}\left\{1 - \frac{3m_{ud}\Sigma}{16\pi^2 F_{\rm phys}^4}\ln\left(\frac{2m_{ud}\Sigma}{F_{\rm phys}^2 M_{\rm phys}^2}\right) + \frac{4m_{ud}\Sigma}{F_{\rm phys}^4} l\right\}, \tag{1}$$

where Σ denotes the chiral condensate, $l = l_3^r - l_7^r + h_1^r - h_3^r$ is a combination of the low-energy constants at next-to-leading order (NLO) [6], and $M_{\rm phys}(= 135$ MeV) and $F_{\rm phys}(= 92$ MeV) are the physical values of the pion mass and decay constant, respectively. Here l_i^r are renormalized at $M_{\rm phys}$. In the formula, we have assumed that the strange quark is decoupled from the theory and $SU(2)$

Funded by SCOAP[3]

chiral perturbation theory works. In other words, the strange quark mass dependence is assumed to be absorbed in the low-energy constants.

By taking a ratio with the ChPT predictions for the pion mass and decay constant (let us denote them by M_π and F_π), one can eliminate the chiral logarithm in Eq. (1):

$$\frac{\chi_t}{M_\pi^2 F_\pi^2} = \frac{1}{4}\left[1 + \frac{2M_\pi^2 l'}{F_\pi^2}\right], \tag{2}$$

where $l' = -l_4^r - l_7^r + h_1^r - h_3^r$ is again a combination of the NLO low-energy constants, which is independent of the renormalization scheme and scale at this order. This ratio also cancels possible finite volume effects at NLO. Moreover, the chiral limit of the ratio, 1/4, is protected from the strange sea quark effects (see Appendix A for details), as they always enter as a function of the ratio m_{ud}/m_s, which can be absorbed into the (finite) renormalization of l'. We can therefore precisely estimate the topological susceptibility at the physical point by measuring χ_t, M_π, and F_π at each simulation point.

It has been a challenging task for lattice QCD to compute χ_t, since it is sensitive to the discretization effects and the violation of chiral symmetry [7–9] in particular. This is partly because the quark mass dependence of χ_t is due to sea quarks, or a small quantum mechanical effect suppressed by $O(\hbar)$, to which the discretization error is relatively large. Even if we could simulate QCD on a sufficiently fine lattice, the global topological charge would become frozen along the Monte Carlo history [10]. Due to these difficulties, the study of the quark mass dependence and its comparison with the ChPT formula of χ_t has been very limited, and only some pilot works with dynamical chiral fermions on rather small or coarse lattices [11–19] are available.

In this work, we improve the computation of χ_t in two ways. One is to employ the domain-wall fermion [20,21] with an improvement by Refs. [22,23], known as the Möbius domain-wall fermion, for the dynamical quarks, which enables us to precisely preserve chiral symmetry. Even on our coarsest lattice, the residual mass, related to the violation of the chiral symmetry, is kept at the order of 1 MeV. As will be shown below, our results show only a mild dependence of χ_t on the lattice spacing, up to $a \sim 0.08$ fm. The use of the domain-wall fermion allows us to sample configurations in different topological sectors, which is also an advantage over the simulation with the overlap fermion where we fixed the global topological charge in Ref. [12].

Another improvement comes from the use of sub-volumes of the simulated lattices. Since the correlation length of QCD is limited, at most by $1/M_\pi$, there is essentially no need to use the global topological charge to compute χ_t. The use of sub-volume was tested in our previous simulations with overlap quarks [12,16] (see also Refs. [24,25]), where the signal was extracted from finite volume effects, which have some sensitivity to χ_t [26,27]. In this work, we utilize a different method, which was originally proposed by Bietenholz et al. [28,29] (similar methods were proposed in Refs. [30] and [31]). The method is based on a correlator, which gives a positive finite value even in the thermodynamical limit, and thus is less noisy than our recent attempt in Ref. [32][1]. We confirm that 30%–50% sub-volumes of the whole lattice, whose size is ~ 2 fm, are sufficient to extract χ_t. Moreover, the new definition shows more frequent fluctuation than that of the global topological charge on our finest lattice.

We also employ a modern technique, the Yang–Mills (YM) gradient flow [34–36], in order to make the global topological charge close to integers, to remove the UV divergences, and to reduce the

[1] See also Ref. [33], where a similar method to ours was attempted.

statistical noise. With these improvements, we achieve good enough statistical precision to investigate the dependence of χ_t on the sea quark mass. In fact, our data of the topological susceptibility are consistent with the ChPT prediction (1), from which the values of chiral condensate and l' are extracted.

The same set of data was also used to calculate the η' meson mass [37], which was extracted from the shorter distance region of the correlator of the topological charge density. These two results show a nontrivial double-scale structure of topological fluctuation of the gauge field: it creates the η' meson at short distances, while describing the vacuum mode of the pion (or the lowest mode, which is constant over space-time) at long distances.

The rest of this paper is organized as follows. First, we describe our lattice setup in Sect. 2. We then explain the method to extract the topological susceptibility from the slab sub-volume in Sect. 3. Our results at lower β are presented in Sect. 4. Comparing the data with those obtained from global topology, we examine the validity of our sub-volume method. The results at higher β are shown in Sect. 5, and how we estimate the statistical errors is explained in Sect. 6. Finally, we estimate the chiral and continuum limits in Sect. 7 and give a summary in Sect. 8.

2. Lattice setup

In the numerical simulation[2] of QCD, we use the Symanzik gauge action and the Möbius domain-wall fermion action for gauge ensemble generations [38–41]. We apply three steps of stout smearing of the gauge links [42] for the computation of the Dirac operator. Our main runs of $2+1$-flavor lattice QCD simulations are performed with two different lattice sizes $L^3 \times T = 32^3 \times 64$ and $48^3 \times 96$, for which we set $\beta = 4.17$ and 4.35, respectively. The inverse lattice spacing $1/a$ is estimated to be 2.453(4) GeV (for $\beta = 4.17$) and 3.610(9) GeV (for $\beta = 4.35$), using the input $\sqrt{t_0} = 0.1465$ fm [43] where we use the reference YM gradient flow–time t_0, defined by $t^2\langle E\rangle|_{t=t_0} = 0.3$ [34] with the energy density E of the gluon field. The two lattices share a similar physical size $L \sim 2.6$ fm. For the quark masses, we choose two values of the strange quark mass m_s around its physical point, and 3–4 values of the up and down quark masses m_{ud} for each m_s. Since our data at the lightest pion mass around 230 MeV ($am_{ud} = 0.0035$ at $\beta = 4.17$) may contain significant finite size effects, we simulate a larger lattice $48^3 \times 96$ with the same set of parameters to check if the finite volume systematics is small enough. We also perform a simulation on a finer lattice $64^3 \times 128$ (at $\beta = 4.47$ [$1/a \sim 4.5$ GeV] and $M_\pi \sim 285$ MeV). For each ensemble, 500–1000 gauge configurations are sampled from 5000 molecular dynamics (MD) time. The ensembles used in this work are listed in Table 1.

In this setup, we confirm that the violation of the chiral symmetry in the Möbius domain-wall fermion formalism is well under control. The residual mass is ~ 1 MeV [44] by choosing the lattice size in the fifth direction $L_5 = 12$ at $\beta = 4.17$ and less than 0.2 MeV with $L_5 = 8$ at $\beta = 4.35$ (and 4.47).

On generated configurations, we perform 500–1640 steps of the YM gradient flow (using the conventional Wilson gauge action) with a step-size $\Delta t/a^2 = 0.01$. At every 200–400 steps (depending on the parameters) we store the configuration of the topological charge density. The two-point correlator is measured using the fast Fourier transform (FFT) technique to average source and sink points over whole lattice sites.

In the following analysis, we measure the integrated auto-correlation time of every quantity, following the method proposed in Refs. [10,45]. The statistical error is estimated by the jackknife method

[2] Numerical works are done with the QCD software package IroIro++ [40,41].

Table 1. Parameters of the JLQCD gauge ensembles used in this work. Pion masses are rounded to the nearest 10 MeV.

Lattice spacing	$L^3 \times T$	L_5	am_{ud}	am_s	m_π [MeV]	$m_\pi L$
$\beta = 4.17$,	$32^3 \times 64$ ($L = 2.6$ fm)	12	0.0035	0.040	230	3.0
$a^{-1} = 2.453(4)$ GeV			0.0070	0.030	310	4.0
			0.0070	0.040	310	4.0
			0.0120	0.030	400	5.2
			0.0120	0.040	400	5.2
			0.0190	0.030	500	6.5
			0.0190	0.040	500	6.5
	$48^3 \times 96$ ($L = 3.9$ fm)	12	0.0035	0.040	230	4.4
$\beta = 4.35$,	$48^3 \times 96$ ($L = 2.6$ fm)	8	0.0042	0.018	300	3.9
$a^{-1} = 3.610(9)$ GeV			0.0042	0.025	300	3.9
			0.0080	0.018	410	5.4
			0.0080	0.025	410	5.4
			0.0120	0.018	500	6.6
			0.0120	0.025	500	6.6
$\beta = 4.47$,	$64^3 \times 128$ ($L = 2.7$ fm)	8	0.0030	0.015	280	4.0
$a^{-1} = 4.496(9)$ GeV						

(without binning) multiplied by the square root of auto-correlation time normalized by the MD time interval of the configuration samples. We will discuss more details about the auto-correlation time of topological fluctuations in Sect. 6.

The pion mass and decay constant are computed combining the pseudoscalar correlators with local and smeared source operators. Details of the computation are presented in a separate article [46].

3. Topological susceptibility in a "slab"

We use the conventional gluonic definition of the topological charge density $q^{\rm lat}(x)$, the so-called clover construction [9]. Since the YM gradient flow smooths the gauge field in the range of $\sqrt{8t} \sim 0.5$ fm of the lattice, a simple summation $Q_{\rm lat} = \sum_x q^{\rm lat}(x)$ over the whole sites gives values close to integers, as shown in Fig. 1.

As is well known, the global topological charge $Q_{\rm lat}$ suffers from long auto-correlation time in lattice simulations, especially when the lattice spacing is small. This is also true in our simulations,

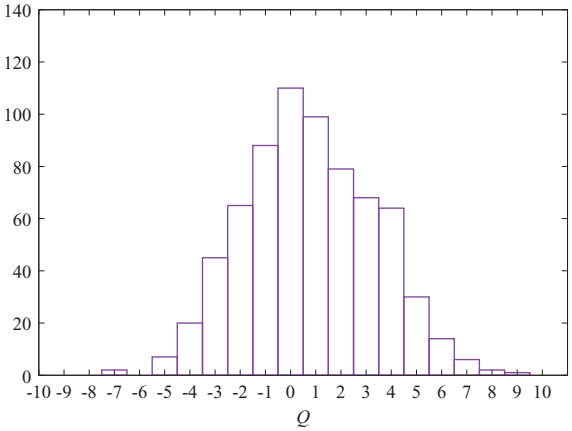

Fig. 1. The distribution of $\sum_x q^{\rm lat}(x)$ at $\beta = 4.17$, $m_{ud} = 0.007$, and $m_s = 0.04$.

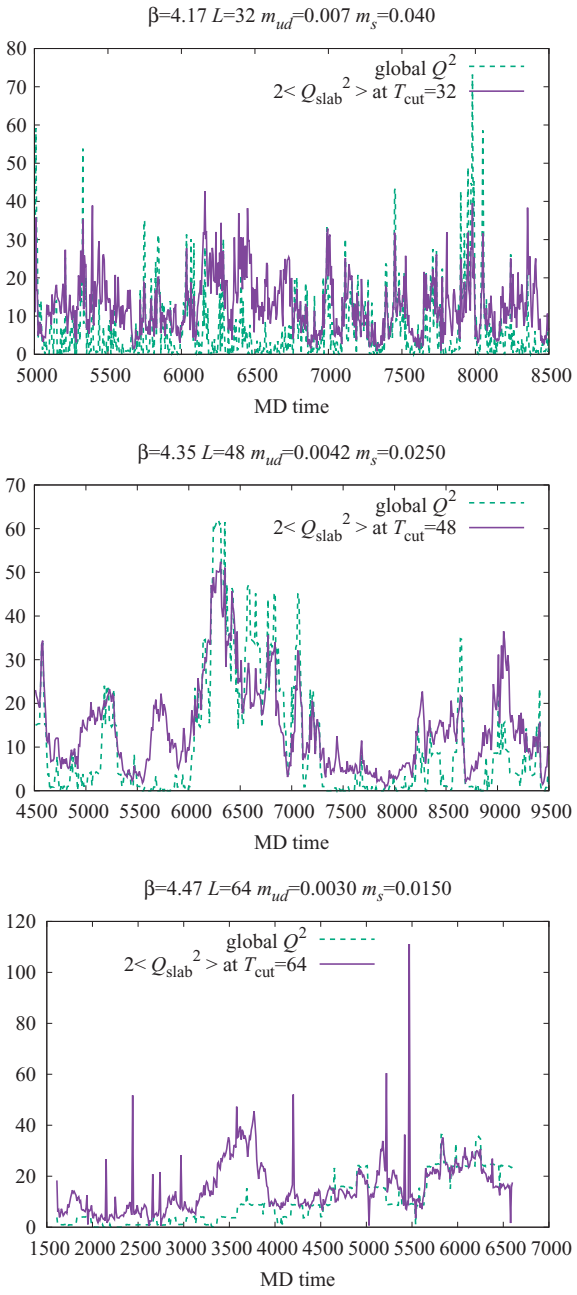

Fig. 2. MD history of $\langle Q^2_{\rm slab}(T_{\rm cut} = T/2)\rangle$ (solid lines) and that of global topological charge Q^2 (dashed). Data at $\beta = 4.17$, $m_{ud} = 0.007$, $m_s = 0.040$ (top panel) and those at $\beta = 4.35$, $m_{ud} = 0.0042$, $m_s = 0.0250$ (middle) and at $\beta = 4.47$, $m_{ud} = 0.0030$, $m_s = 0.0150$ (bottom) are shown. These three simulations share a similar value of the pion mass $\sim$ 300 MeV and physical volume.

as shown in Fig. 2. At the highest $\beta = 4.47$, $Q_{\rm lat}$ drifts very slowly with an auto-correlation time of possibly $O(1000)$. It is, therefore, not feasible to estimate χ_t without performing much longer runs. The details of the auto-correlation time of the topological charge and its density operator will be discussed in Sect. 6.

Instead of using the global topological charge $Q_{\rm lat}$, we attempt to extract the topological susceptibility from a sub-volume $V_{\rm sub}$ of the whole lattice V. Since the correlation length of QCD is limited by at most $1/M_\pi$, the sub-volume $V_{\rm sub}$ should contain sufficient information to extract χ_t, provided

that its size is larger than $1/M_\pi$. One can then effectively increase the statistics by $V/V_{\rm sub}$, since each piece of $V/V_{\rm sub}$ sub-lattices may be considered as an uncorrelated sample. Moreover, there is no potential barrier among topological sectors: the instantons and anti-instantons freely come in and go out of the sub-volume, which should make the auto-correlation time of the observable shorter than that of the global topological charge.

There are various ways of cutting the whole lattice into sub-volumes and computing the correlation functions in them. After some trial and error, we find that the so-called "slab" method, proposed by Bietenholz et al. [28], is efficient for the purpose of computing χ_t. The idea is to sum up the two-point correlators of the topological charge density, over x and y in the same sub-volume:

$$\langle Q^2_{\rm slab}(T_{\rm cut})\rangle \equiv \int_{T_{\rm ref}}^{T_{\rm cut}+T_{\rm ref}} dx_0 \int_{T_{\rm ref}}^{T_{\rm cut}+T_{\rm ref}} dy_0 \int d^3x \int d^3y \left\langle q^{\rm lat}(x) q^{\rm lat}(y)\right\rangle. \tag{3}$$

Here the integration over x and y in the spatial directions runs in the whole spatial volume (since the YM gradient flow is already performed, there is no divergence from the points of $x = y$), while the temporal sum is restricted to the region $[T_{\rm ref}, T_{\rm cut} + T_{\rm ref}]$, which is called a "slab". Here $T_{\rm ref}$ is an arbitrary reference time. Due to the translational invariance, slabs sharing the same thickness $T_{\rm cut}$ are physically equivalent, and one can average over $T_{\rm ref}$. This method is statistically more stable than the other sub-volume method that we applied in Refs. [12,16] because $\langle Q^2_{\rm slab}(T_{\rm cut})\rangle$ is guaranteed to be always positive.

If we sample large statistics on a large enough lattice volume, $\langle Q^2_{\rm slab}(T_{\rm cut})\rangle$ should be just $T_{\rm cut}/T$ of $\chi_t V$. Namely, $\langle Q^2_{\rm slab}(T_{\rm cut})\rangle$ should be a linear function in $T_{\rm cut}$. Its leading finite volume correction can be estimated using the formula in Ref. [27]:

$$\langle Q^2_{\rm slab}(T_{\rm cut})\rangle = (\chi_t V) \times \frac{T_{\rm cut}}{T} + C(1 - e^{-m_0 T_{\rm cut}})(1 - e^{-m_0 (T - T_{\rm cut})}), \tag{4}$$

where C is an unknown constant, and m_0 is the mass of the first excited state, the η' meson[3]. Note that for $1/m_0 \ll T_{\rm cut} \ll T - 1/m_0$, the formula gives a simple linear function in $T_{\rm cut}$ plus a constant. Also, note that in the limit of $T_{\rm cut} = T$, $\langle Q^2_{\rm slab}(T_{\rm cut} = T)\rangle = \langle Q^2\rangle = \chi_t V$.

Assuming the linearity in $T_{\rm cut}$, one can extract the topological susceptibility through

$$\chi_t^{\rm slab} = \frac{T}{V}\left[\frac{\langle Q^2_{\rm slab}(t_1)\rangle - \langle Q^2_{\rm slab}(t_2)\rangle}{t_1 - t_2}\right], \tag{5}$$

with two reference thicknesses t_1 and t_2. In our numerical analysis, $T_{\rm ref}$ is averaged over the temporal direction. Since the data at t_i and $T - t_i$ are not independent, we choose t_1 and t_2 in a range 1.6 fm $< t_1, t_2 < T/2$. In the numerical analysis, we replace $q^{\rm lat}(x)$ by $q^{\rm lat}(x) - \langle Q_{\rm lat}/V\rangle$ to cancel a possible bias due to the long auto-correlation of the global topology.

The original proposal in Ref. [28] mainly used the correlator in a fixed topological sector. The formula corresponding to Eq. (4) then contains a subtraction of the contribution from the global topology. We find that the statistical noise is larger with this choice while the results from different topological sectors are consistent. In the following analysis, we use Eq. (4) after summing over the topological sectors.

[3] The finite volume effects are due to propagation of the mesons in the flavor singlet channel. As the ground state or the η' meson is heavy, we neglect the higher-order effects. Even if we include them, the structure of linear + constant in Eq. 4 is unchanged since their effect is just an additional constant.

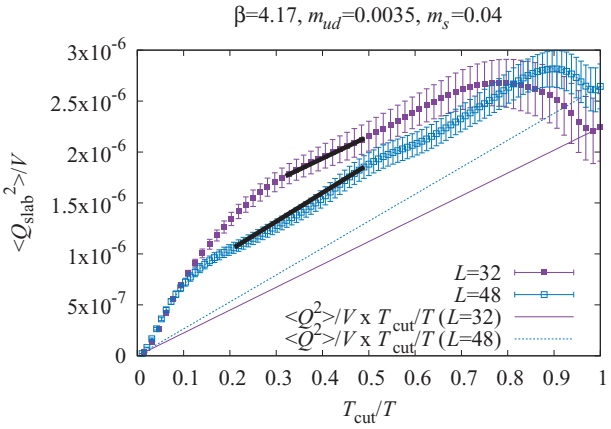

Fig. 3. $\langle Q^2_{\rm slab}(T_{\rm cut})\rangle$ as a function of $T_{\rm cut}/T$. Data at the lightest mass $m_{ud} = 0.0035$, $\beta = 4.17$ with two different lattice sizes $L = 32$ and $L = 48$ are shown. $T = 2L$ for both lattices. The solid and dotted lines show the slope obtained from the global topological charge measured on the $L = 32$ and $L = 48$ lattices, respectively. Two end-points of the thick line segments show the reference points t_1 and t_2 taken for determination of the topological susceptibility. Note that the value of $t_1 = 20$ is the same for the two data.

We find that the signal using this slab method is less noisy than the previous attempts in Refs. [12,16]. Moreover, as shown in Fig. 2 and discussed in detail later, the new definition shows more frequent fluctuation than that of the global topological charge on our finest lattice.

4. Results at low β

At $\beta = 4.17$, which corresponds to the lattice spacing $a \sim 0.08$ fm, both the global topological charge $Q_{\rm lat}$ and $Q^2_{\rm slab}(T_{\rm cut})$ fluctuate well, as shown in the top panel of Fig. 2. The data on this lattice, therefore, provide a good testing ground to examine the validity of the slab sub-volume method, compared with the naive definition of the topological susceptibility with $\langle Q^2_{\rm lat}\rangle/V$.

In Fig. 3, $\langle Q^2_{\rm slab}(t_{\rm cut})\rangle$ observed at the lightest sea quark mass $m_{ud} = 0.0035$, $\beta = 4.17$ on two different volumes $L = 32$ and $L = 48$ is plotted as a function of $T_{\rm cut}/T$. The data converge to a linear plus constant function given in Eq. (4) at $T_{\rm cut} = 20$, which corresponds to ~ 1.6 fm. The slope, or $\chi_t^{\rm slab}$, is consistent with that from global topology, shown by solid and dotted lines for the $L = 32$ and $L = 48$ lattices, respectively. We also observe the consistency between the $L = 32$ and $L = 48$ data, which suggests that the systematics due to the finite volume is well under control.

The "linear + constant" behavior is also seen in ensembles with heavier quark masses, as presented in Fig. 4.

The extracted values of the topological susceptibility from the slope show a good agreement with the ChPT prediction, as shown in Fig. 5 by open and filled squares. The leading-order ChPT formula, $\chi_t = m_{ud}\Sigma/2$, with $\Sigma = [270\,{\rm MeV}]^3$ (solid line) is shown to guide the eye. In the same plot, we also plot the estimate for χ_t obtained from the global topological charge by circles, which again agrees with the results, validating the slab method. The values of $\chi_t^{\rm slab}$ are listed in Table 2. How we estimate their error bars is explained in the following two sections.

5. Results at high beta

At higher β values, we still find a reasonable slope at the lightest quark mass for each β and m_s, as shown in Fig. 6. For heavier masses, however, some curvature is seen. We consider this curvature to be an effect from the bias of the global topological charge. This observation is consistent with previous

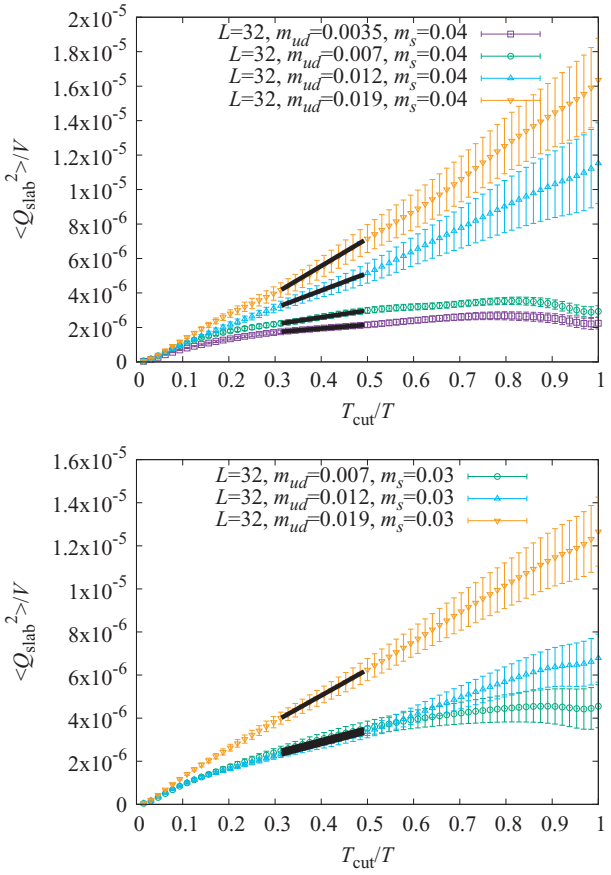

Fig. 4. Same as Fig. 3 but at different up and down quark masses. Data at $\beta = 4.17$ and $m_s = 0.04$ (top panel) and those at $m_s = 0.03$ (bottom) are shown.

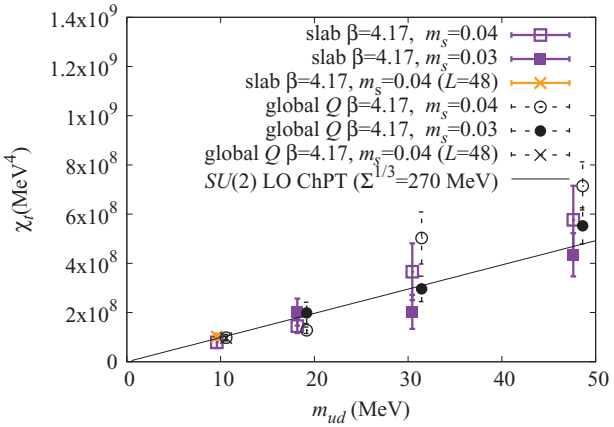

Fig. 5. m_{ud} dependence of topological susceptibility at $\beta = 4.17$ obtained from $\langle Q^2_{\rm slab}(T_{\rm cut})\rangle$ (solid symbols) and those from the global topological charge (dashed, slightly shifted to avoid overlapping with the former data). The LO prediction from $SU(2)$ ChPT, where the chiral condensate $\Sigma^{1/3} = 270$ MeV, is also shown to guide the eye.

works (see, e.g., Ref. [10]), which reported that heavier pion mass ensembles show the longer autocorrelation of the topological charge, and the larger deviation of $\langle Q_{\rm lat}\rangle$ from zero. We determine the reference $t_1 \sim 1.6$ fm using data at the lightest quark mass and always choose $t_2 = T/2 \sim 2.6$ fm. In order to estimate the systematic errors due to nonlinear behavior, we compare the results

Table 2. Results for the pion mass M_π, decay constant $\sqrt{2}F_\pi$, $\tau_{\rm exp}$, $\tau_{\rm imp}$, and $\chi_t^{\rm slab}$. $\tau_{\rm exp}$ for $\beta = 4.47$ is estimated from the first zero-crossing point of $Q_{\rm lat}$. All the data are shown in lattice units. For $\chi_t^{\rm slab}$, the first error denotes the statistical error, while the second shows the systematic error due to the effect of freezing the global topological charge.

β	L	m_{ud}	m_s	M_π	$\sqrt{2}F_\pi$	$\tau_{\rm exp}$	$\tau_{\rm imp}$	$\chi_t^{\rm slab}$
4.17	32	0.0035	0.04	0.093 69(32)	0.053 20(19)	17(04)	25(9)	$0.217(64)(14)\times10^{-5}$
		0.007	0.04	0.126 04(26)	0.057 74(15)	14(03)	30(9)	$0.400(78)(21)\times10^{-5}$
		0.012	0.04	0.162 67(22)	0.062 54(14)	65(40)	62(24)	$1.01(32)(46)\times10^{-5}$
		0.019	0.04	0.203 29(19)	0.067 88(14)	65(40)	56(22)	$1.59(38)(09)\times10^{-5}$
		0.007	0.03	0.126 29(26)	0.057 61(15)	29(07)	54(22)	$0.56(15)(53)\times10^{-5}$
		0.012	0.03	0.161 79(21)	0.061 90(14)	74(50)	71(32)	$0.56(19)(22)\times10^{-5}$
		0.019	0.03	0.203 02(20)	0.067 30(13)	56(35)	42(16)	$1.20(24)(23)\times10^{-5}$
	48	0.0035	0.04	0.092 03(09)	0.054 40(09)	38(30)	21(06)	$0.282(34)(42)\times10^{-5}$
4.35	48	0.0042	0.025	0.082 99(18)	0.039 26(11)	243(153)	208(114)	$0.91(40)(12)\times10^{-6}$
		0.0080	0.025	0.113 12(14)	0.042 91(09)	318(200)	362(234)	$2.18(98)(48)\times10^{-6}$
		0.0120	0.025	0.138 75(14)	0.046 30(08)	173(142)	105(52)	$1.21(32)(07)\times10^{-6}$
		0.0042	0.018	0.082 19(19)	0.039 01(11)	111(49)	158(72)	$0.59(37)(12)\times10^{-6}$
		0.0080	0.018	0.112 84(15)	0.042 75(08)	236(148)	220(126)	$0.55(53)(19)\times10^{-6}$
		0.0120	0.018	0.137 99(13)	0.046 03(09)	97(43)	170(82)	$1.70(53)(21)\times10^{-6}$
4.47	64	0.0030	0.015	0.063 16(15)	0.031 41(09)	[1700]	492(836)	$0.20(27)(09)\times10^{-6}$

with 1) those obtained from different reference times $(t_1', t_2') = (t_1, \frac{t_1+t_2}{2})$, and $(\frac{t_1+t_2}{2}, t_2)$, and 2) those obtained without the subtraction of $\langle Q\rangle/V$ in the definition of the topological charge density. The larger deviation is treated as a systematic error. More details are presented in Appendix B.

Our results are summarized in Fig. 7 (see also Fig. 8 for a comparison with Refs. [8] and [9]). Although the data at higher β are rather scattered compared to those at $\beta = 4.17$, they can be used to estimate the chiral condensate Σ, assuming the linear suppression around the chiral limit. Before going to the details, we discuss the auto-correlation of $\chi_t^{\rm slab}$ and show how we estimate the statistical errors in the next section.

6. Auto-correlation and error estimates

Gauge configurations generated by a Markov chain are generally not independent but have auto-correlations. How much they are correlated depends on the observables. We therefore need to carefully measure the auto-correlation of the target observable O:

$$\Gamma_O(\Delta\tau) = \langle O(\tau)O(\tau+\Delta\tau)\rangle_\tau, \tag{6}$$

where τ denotes the Monte Carlo time, and the average $\langle\cdots\rangle_\tau$ is taken over τ.

When the Monte Carlo trajectory is long enough, compared to the auto-correlation time of any observables, one can estimate the so-called integrated auto-correlation time by

$$\tau_{\rm int} = \frac{1}{2} + \sum_{\Delta\tau=0}^{W} \rho(\Delta\tau), \quad \rho(\Delta\tau) = \frac{\Gamma_O(\Delta\tau)}{\Gamma_O(0)}, \tag{7}$$

where the upper end of the summation window W is chosen to where $\rho(\Delta\tau)$ becomes consistent with zero within the error. The above formula assumes that $\Gamma_O(\Delta\tau)$ converges to a single exponential function well below W.

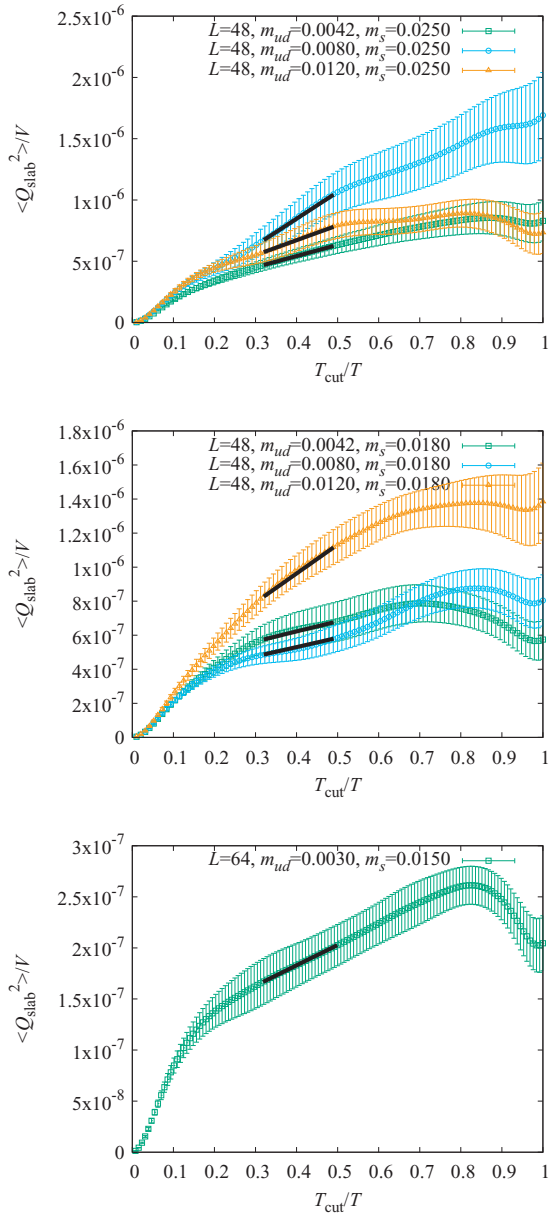

Fig. 6. $\langle Q^2_{\rm slab}(T_{\rm cut})\rangle$ at different up and down quark masses. Data at $\beta = 4.35$ and $m_s = 0.0180$ (top) and $m_s = 0.0250$ (middle) and those at $\beta = 4.47$ and $m_s = 0.0150$ (bottom) are shown.

If the observables suffer from long auto-correlation, and the Monte Carlo trajectory is not long enough, on the other hand, the above procedure may underestimate the auto-correlation time, since some very slow decay modes can be hidden in the error of $\rho(\Delta\tau)$. This problem is similar to that of hadron spectroscopy with a short temporal extension, where one does not have a long enough fitting range to disentangle the ground state from excited states, which leads to over-estimation of the mass.

The ALPHA Collaboration [10] carefully studied the effect of slow modes, and proposed an improved estimate of the auto-correlation time,

$$\tau_{\rm imp} = \tau'_{\rm int} + \tau_{\rm exp}\rho(W'), \tag{8}$$

where $\tau'_{\rm int}$ is the same summation as Eq. (7) but with a smaller upper bound W' where $\rho(W')$ becomes lower than 3/2 standard deviations. $\tau_{\rm exp}$ is the auto-correlation of the slowest mode. The proposal is

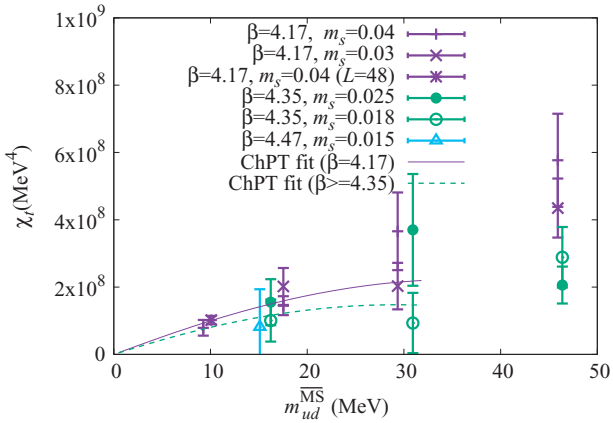

Fig. 7. m_{ud} dependence of topological susceptibility obtained from the slab sub-volume method. The heaviest four points are not included in the fit.

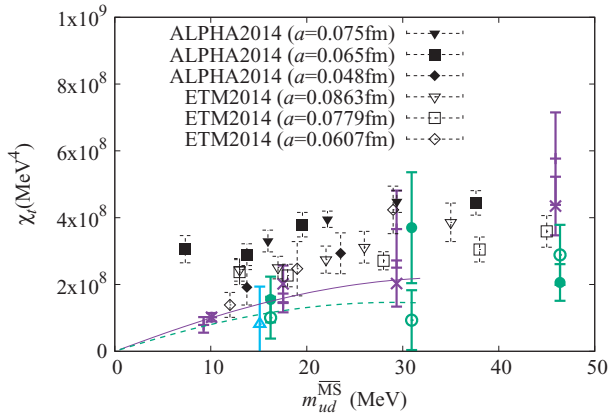

Fig. 8. The same figure as Fig. 7 but a comparison with Ref. [8] (ETM2014, $N_f = 2+1+1$ results converted using the input $r_0 = 0.46$ fm) and Ref. [9] (ALPHA2014, $N_f = 2$ results converted assuming $m_{ud} = M_\pi^2 F_\pi^2/(2\Sigma)$ using the inputs $t_1 = 0.061$ fm^2, $F_\pi = 92$ MeV, and $\Sigma = (270\ \text{MeV})^3$) is shown.

equivalent to considering a continuation of $\Gamma_O(\Delta\tau)$ at $\Delta\tau = W'$ to the slowest possible exponential function $\Gamma_O(W')\exp(-(\Delta\tau - W')/\tau_{\rm exp})$.

In lattice QCD simulations, it is natural to assume that $\tau_{\rm exp}$ is equal to the auto-correlation of the global topological charge. In our simulations, $\tau_{\rm exp}$ is estimated by $\tau_{\rm int}(W)$ of $Q_{\rm lat}^2$, except for $\beta = 4.47$ where we choose $\tau_{\rm exp} = 1700$ MD time by hand (and assuming 100% error for it), which is a rough order estimate from the first zero-crossing point of $Q_{\rm lat}$. Then we compute the auto-correlation of our target observable $\chi_t^{\rm slab}$ by $\tau_{\rm imp}$ to estimate the error. The results for $\tau_{\rm imp}$, $\tau_{\rm exp}$, and $\chi_t^{\rm slab}$ are summarized in Table 2 and the auto-correlation function $\rho(\Delta\tau)$ at three different β with a similar pion mass $M_\pi \sim 300$ MeV is shown in Fig. 9. At the highest $\beta = 4.47$, it is clear that $\chi_t^{\rm slab}$ has a shorter auto-correlation time than that of the global topological charge.

With the measured improved auto-correlation time $\tau_{\rm imp}$, we estimate the statistical errors of $\chi_t^{\rm slab}$ by multiplying $\sqrt{2(\tau_{\rm imp} + \Delta\tau_{\rm imp})/\tau_{\rm interval}}$ to the naive error estimates, where $\Delta\tau_{\rm imp}$ is the standard deviation of $\tau_{\rm imp}$ and $\tau_{\rm interval}$ denotes the interval trajectory between samples. The results, as well as the systematic error from the choice of reference points, are listed in the last column of Table 2.

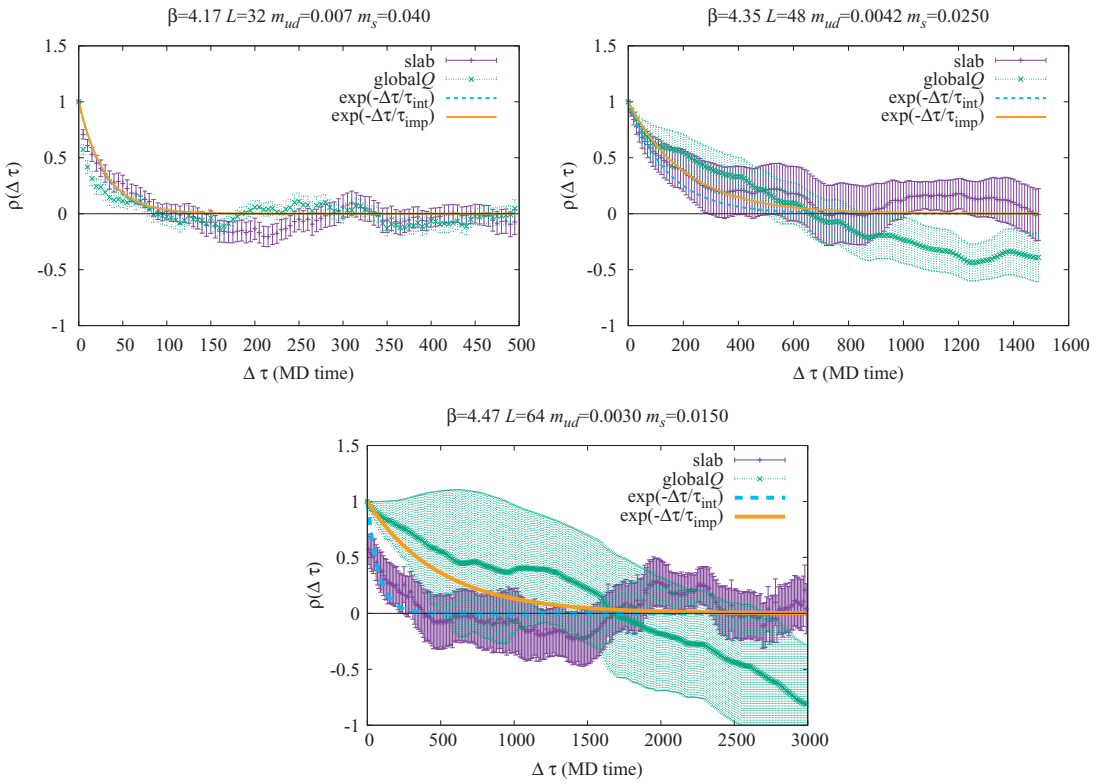

Fig. 9. Auto-correlation function $\rho(\Delta\tau)$ of $\chi_t^{\rm slab}$ (pluses) and $Q^2_{\rm lat}$ (crosses) at three different β with a similar pion mass $M_\pi \sim 300$ MeV.

7. Chiral and continuum limit

Figure 7 presents our data for $\chi_t^{\rm slab}$ from all ensembles plotted in physical units. The horizontal axis, the quark mass defined in the $\overline{\rm MS}$ scheme at 2 GeV, is

$$m_{ud}^{\overline{\rm MS}} = (m_{ud} + m_{\rm res})/Z_S, \tag{9}$$

where the renormalization factor Z_S is nonperturbatively computed in Ref. [48]: $Z_S = 1.037,\ 0.934,$ and 0.893 for $\beta = 4.17,\ 4.35,$ and 4.47, respectively. In contrast to the results by other groups with non-chiral fermions, we find no strong dependence on β.

First, we compare our results directly to the ChPT formula (1). We perform a two-parameter (Σ and l) fit to the data at $\beta = 4.17$ (solid curve in Fig. 7) and $\beta \geq 4.35$ (dashed curve) separately[4]. The results for Σ and l are listed in Table 3. Here we also perform the same fit but omitting the heaviest two points, and take the difference as an estimate for the systematic error in the chiral extrapolation. Since the heaviest points have several problems—1) a strong bias is seen in the global topology, 2) ChPT is less reliable, and 3) there is mismatch between different β—we take the result without them as our central values. Note, however, that this inclusion/elimination affects l but Σ is stable against the change in the fit-range. Namely, the chiral condensate Σ is determined by the low quark mass data. We then estimate the continuum limit by a constant fit, as shown in the top two

[4] Since $\beta = 4.47$ is simulated at only one choice of the quark masses, we simply add the data as one of the $\beta = 4.35$ ensembles. In fact, the χ_t values at $\beta = 4.35$ and 4.47 at the pion mass ~ 300 MeV are consistent with each other.

Table 3. Our results for Σ, l, l', and $\chi_t^{\rm slab}/(M_\pi F_\pi)^2$ at the physical point. The first error denotes the the statistic fluctuation at each simulation point, including the effect of long auto-correlation of global topology. The second is the systematic error in chiral extrapolation, and the third error denotes that in the continuum limit estimates. See the main text for details.

β	$\Sigma^{1/3}$(MeV)	l	l'	$\frac{\chi_t^{\rm slab}}{M_\pi^2 F_\pi^2}$ at physical point
4.17	275(13)(13)	0.003(06)(10)	−0.018(03)(03)	0.232(04)(03)
$\geq$ 4.35	261(50)(19)	−0.005(09)(06)	−0.025(05)(04)	0.223(05)(04)
continuum limit	274(13)(25)(15)	−0.001(05)(06)(19)	−0.019(03)(01)(13)	0.229(03)(01)(13)

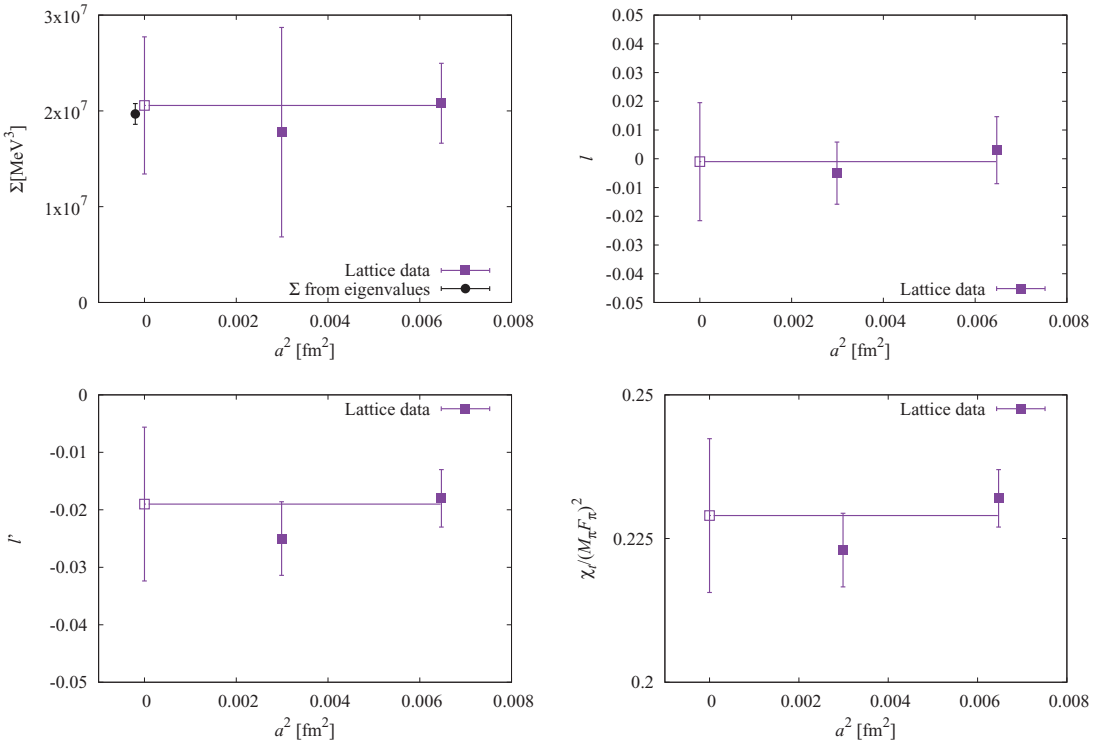

Fig. 10. Continuum limit of Σ (we also plot our recent result [49] obtained from the Dirac eigenvalue density), l, l', and $\chi_t^{\rm slab}/(M_\pi F_\pi)^2$ estimated by a constant fit at the physical point.

panels in Fig. 10. Comparing our result from the constant fit with linear extrapolation of the central values, we take the difference as an estimate for the systematic error in the continuum limit. In the plots in Fig. 10, all these errors are added in quadrature.

Next, using our data for the pion mass M_π and decay constant F_π together with $\chi_t^{\rm slab}$, obtained from each ensemble, we take the ratio given in Eq. (2). By a linear one-parameter fit, we determine l' and the ratio $\chi_t^{\rm slab}/(M_\pi F_\pi)^2$ at the physical point. In the same way as the determination of Σ and l, we take the chiral and continuum limits of both quantities. Note that the fixed chiral limit at $1/4$ of the ratio helps us to determine these quantities.

Finally let us discuss other possible systematic effects. In our analysis, the ensembles satisfying $M_\pi L > 3.9$ are used and we do not expect any sizable finite volume effects. In particular, our lightest mass point has $M_\pi L = 4.4$. We have used configurations at the YM gradient flow–time around $\sqrt{8t} \sim 0.5$ fm. We confirm that the flow–time dependence is negligible in the range 0.25 fm

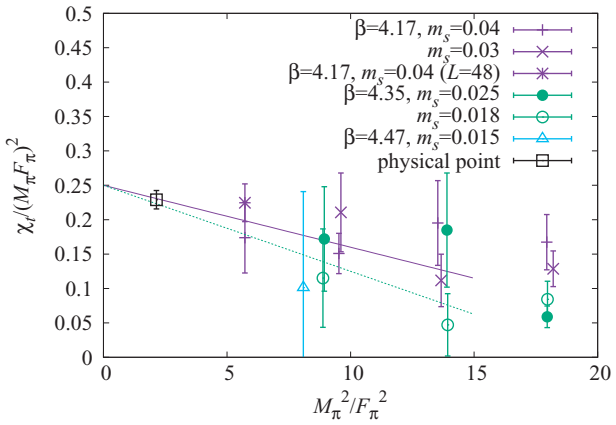

Fig. 11. m_{ud} dependence of the ratio $\frac{\chi_t}{M_\pi^2 F_\pi^2}$. The data at $M_\pi^2/F_\pi^2 > 15$ are not included in the fit.

$< \sqrt{8t} < 0.5$ fm. We conclude that all these systematic effects are negligibly small compared to the statistical and systematic errors given above.

8. Summary

With dynamical Möbius domain-wall fermions and the new method using a sub-volume of the simulated lattice, we have computed the topological susceptibility of QCD. Its quark mass dependence is consistent with the ChPT prediction, from which we have obtained

$$\chi_t = 0.229(03)(01)(13) M_\pi^2 F_\pi^2 \text{ (at physical point)}, \tag{10}$$

$$\Sigma^{\overline{\text{MS}}}(2\,\text{GeV}) = [274(13)(25)(15)\,\text{MeV}]^3, \tag{11}$$

where the first error comes from the statistical uncertainty at each simulation point, including the effect of freezing topology. The second and third errors represent the systematics in the chiral and continuum limits, respectively. The value of Σ is consistent with our recent determination through the Dirac spectrum [49]. We have also estimated the NLO coefficient

$$l = (l_3^r - l_7^r + h_1^r - h_3^r) = -0.001(05)(06)(19), \tag{12}$$

$$l' = (-l_4^r - l_7^r + h_1^r - h_3^r) = -0.019(03)(01)(13), \tag{13}$$

where l is renormalized at the physical pion mass, while l' is renormalization invariant. It is interesting to note that l and l' include a combination of the coefficients $h_1^r - h_3^r$, which are supposed to be *unphysical* in ChPT unless θ dependence is considered. These are important for possible couplings of QCD to axions [50].

Acknowledgements

We thank T. Izubuchi and other members of the JLQCD Collaboration for fruitful discussions. We also thank the Yukawa Institute for Theoretical Physics, Kyoto University. Discussions during the YITP workshop YITP-T-14-03 on "Hadrons and Hadron Interactions in QCD" were useful in completing this work. Numerical simulations were performed on the IBM System Blue Gene Solution at KEK with the support of its Large Scale Simulation Program (No. 16/17-14). This work is supported in part by a Japanese Grant-in-Aid for Scientific Research (Nos. JP25800147, JP26247043, JP26400259, JP16H03978), and by MEXT as "Priority Issue on Post-K computer" (Elucidation of the Fundamental Laws and Evolution of the Universe) and by the Joint Institute for Computational Fundamental Science (JICFuS). The work of G.C. is supported by the STFC, grant ST/L000458/1.

Funding

Open Access funding: SCOAP[3].

Appendix A. Effect of the strange sea quark

In this work, we have assumed that effect of the strange quark is negligible and used $SU(2)$ ChPT in our main analysis to obtain the chiral extrapolation of the topological susceptibility. In this appendix, we consider $SU(3)$ ChPT and compute a possible correction from the strange quark loop. We will show that the chiral limit of the ratio (2) is unchanged even in $SU(3)$ ChPT, which is also protected from finite volume corrections.

The one-loop computation of the topological susceptibility in general N_f-flavor ChPT was given in Refs. [3,4] and the formula for $N_f = 3$ is

$$\chi_t = \bar{m}\Sigma\left[1 + \frac{1}{F_\pi^2}\left\{-3\frac{\bar{m}}{m_{ud}}\Delta(M_\pi^2) - 2\left(\frac{\bar{m}}{m_{ud}} + \frac{\bar{m}}{m_s}\right)\Delta(M_K^2) - \frac{1}{3}\left(\frac{\bar{m}}{m_{ud}} + \frac{2\bar{m}}{m_s}\right)\Delta(M_\eta^2) + 16L_6^r(2M_\pi^2 + M_{ss}^2) + 48(3L_7 + L_8^r)\bar{M}^2\right\}\right], \tag{A.1}$$

where $\bar{m} = m_{ud}m_s/(2m_s + m_{ud})$, M_π,M_K, and M_η are the (simulated) pion, kaon, and η meson masses, respectively. We have also used notations for $M_{ss}^2 = 2m_s\Sigma/F_\pi^2$ and $\bar{M}^2 = 2\bar{m}\Sigma/F_\pi^2$. The chiral logarithm is expressed by

$$\Delta(M^2) = \frac{M^2}{16\pi^2}\ln\frac{M^2}{\mu_{\rm sub}^2} + g_1(M^2), \tag{A.2}$$

where $\mu_{\rm sub}$ denotes the renormalization scale, and g_1 is the finite volume correction (see Ref. [4] for details). In the above formula, we can see three NLO low-energy constants [47]: L_6^r and L_8^r are those renormalized at $\mu_{\rm sub}$, while L_7 is a renormalization scheme independent constant.

One-loop corrections to the pion mass and decay constant were computed in Ref. [47]:

$$M_\pi^2 = M^2\left[1 - \frac{1}{F_\pi^2}\left\{-\frac{1}{2}\Delta(M_\pi^2) + \frac{1}{6}\Delta(M_\eta^2) + 8(L_4^r - 2L_6^r)(2M_\pi^2 + M_{ss}^2) + 8(L_5^r - 2L_8^r)M_\pi^2\right\}\right], \tag{A.3}$$

and

$$F_\pi^2 = F^2\left[1 - \frac{1}{F_\pi^2}\left\{2\Delta(M_\pi^2) + \Delta(M_K^2) - 8L_4^r(2M_\pi^2 + M_{ss}^2) - 8L_5^rM_\pi^2\right\}\right], \tag{A.4}$$

where M and F are the tree-level mass and decay constant, respectively.

Now let us take the ratio of χ_t and $M_\pi^2F_\pi^2$. Noting

$$\bar{m} \sim \frac{m}{2}\left(1 - \frac{m_{ud}}{2m_s}\right) \sim \frac{m}{2}\left(1 - \frac{M_\pi^2}{2M_{ss}^2}\right), \tag{A.5}$$

we obtain

$$\frac{\chi_t}{M_\pi^2F_\pi^2} = \frac{1}{4}\left[1 + \frac{2M_\pi^2l'_{(\rm eff)}}{F_\pi^2} + \mathcal{O}(M_\pi^4)\right], \tag{A.6}$$

where both the strange quark effect as well as finite volume effects from one-loop diagrams are absorbed in the (re)definition of

$$l'_{(\mathrm{eff})} = -\frac{1}{4M_{ss}^2}\left(F_\pi^2 + \Delta(M_K^2) + \frac{1}{2}\Delta(M_\eta^2)\right) + 36L_7 + 4L_8^r. \tag{A.7}$$

We, therefore, conclude that the one-loop formula (2) is valid even when the strange quark gives a nontrivial effect, and is also stable against possible finite volume corrections. This observation helps us in determining χ_t at the physical point.

Appendix B. Bias from global topology

In this appendix, we discuss systematics due to freezing of the global topological charge. Combining the formulas in Refs. [28] and [27], the slab topological charge squared at fixed topology of Q becomes

$$\langle Q^2_{\mathrm{slab}}(T_{\mathrm{cut}})\rangle_Q = (\chi_t V) \times \frac{T_{\mathrm{cut}}}{T} + \frac{T_{\mathrm{cut}}^2}{T^2}\left(Q^2 - \chi_t V\right) + C, \tag{B.1}$$

for $0 \ll T_{\mathrm{cut}} \ll T$. Therefore, if the global topological charge Q were badly sampled and its average of Q^2 in the ensemble deviated from $\chi_t V$, we should have a quadratic term in T_{cut} as

$$\langle Q^2_{\mathrm{slab}}(T_{\mathrm{cut}})\rangle_{\mathrm{biased}} = (\chi_t V)\frac{T_{\mathrm{cut}}}{T}\left[1 + \frac{T_{\mathrm{cut}}}{\chi_t V T}\left(\langle Q^2\rangle_{\mathrm{biased}} - \langle Q\rangle^2_{\mathrm{biased}} - \chi_t V\right)\right] + C, \tag{B.2}$$

where $\langle\cdots\rangle_{\mathrm{biased}}$ denotes the estimate obtained from a biased sampling of configurations. Here we have included the term $\langle Q\rangle^2_{\mathrm{biased}}$, which comes from the use of the subtracted operator $q^{\mathrm{lat}} - \langle Q/V\rangle_{\mathrm{biased}}$ in our numerical analysis.

If the correction $\frac{T_{\mathrm{cut}}}{(\chi_t V)T}\left(\langle Q^2\rangle_{\mathrm{biased}} - \langle Q\rangle^2_{\mathrm{biased}} - \chi_t V\right)$ is small, our original linear + constant formula is still valid. As the correction is proportional to $\frac{T_{\mathrm{cut}}}{T}$, if we have a window $T_{\mathrm{cut}} \ll T$, or the freezing $\langle Q^2\rangle_{\mathrm{biased}} - \langle Q\rangle^2_{\mathrm{biased}}$ happens to be near the true value of $\chi_t V$, we can still extract χ_t from the linear slope (this seems to happen on the data at $\beta = 4.47$).

In order to estimate the systematics due to the correction term, we compare the results with 1) those obtained from different reference times $(t'_1, t'_2) = (t_1, \frac{t_1+t_2}{2})$, and $(\frac{t_1+t_2}{2}, t_2)$,[5] and 2) those obtained without the subtraction of $\langle Q\rangle/V$ in the definition of the topological charge density. Then we take the larger deviation as the systematic error. Since part of $\langle Q\rangle^2_{\mathrm{biased}}$ is expected to be canceled by $\langle Q^2\rangle_{\mathrm{biased}}$, this analysis is rather conservative. As presented in Table 2, the deviations are comparable to the statistical errors.

Let us look into our "worst" case, the data at $\beta = 4.35$ and $(m_{ud}, m_s) = (0.012, 0.018)$ in our ensembles, which shows the strongest curvature. As expected, the global topological charge sampling is biased: the estimate for $\langle Q^2\rangle = 12(4)$ in the former half (0–2500 MD time) of the simulation time is quite different from $\langle Q^2\rangle = 40(17)$ in the latter half (2500–5000 MD time). But the obtained values of χ_t^{slab} show a milder deviation, $1.30(53) \times 10^{-6}$ for the former half and $1.89(64) \times 10^{-6}$ for the latter, which are consistent within errors. This analysis[6] shows that the systematics due to freezing topology is under control, at least, at the level of the statistical errors. Our ChPT fit with reasonable $\chi^2/\mathrm{d.o.f.} \sim 1.4$ also supports our conclusion.

[5] This also tests if the effect from the excited state m_0 is small or not.

[6] We thank W. Bietenholz and P. de Forcrand for suggesting this analysis of freezing topology effects.

References

[1] E. Witten, Nucl. Phys. B **156**, 269 (1979).
[2] G. Veneziano, Phys. Lett. B **95**, 90 (1980).
[3] Y.-Y. Mao and T.-W. Chiu [TWQCD Collaboration], Phys. Rev. D **80**, 034502 (2009) [arXiv:0903.2146 [hep-lat]] [Search INSPIRE].
[4] S. Aoki and H. Fukaya, Phys. Rev. D **81**, 034022 (2010) [arXiv:0906.4852 [hep-lat]] [Search INSPIRE].
[5] F.-K. Guo and U.-G. Meißner, Phys. Lett. B **749**, 278 (2015) [arXiv:1506.05487 [hep-ph]] [Search INSPIRE].
[6] J. Gasser and H. Leutwyler, Ann. Phys. **158**, 142 (1984).
[7] A. Bazavov et al. [MILC Collaboration], Phys. Rev. D **81**, 114501 (2010) [arXiv:1003.5695 [hep-lat]] [Search INSPIRE].
[8] K. Cichy, E. Garcia-Ramos, and K. Jansen [ETM Collaboration], J. High Energy Phys. **02**, 119 (2014) [arXiv:1312.5161 [hep-lat]] [Search INSPIRE].
[9] M. Bruno, S. Schaefer, and R. Sommer [ALPHA Collaboration], J. High Energy Phys. **08**, 150 (2014) [arXiv:1406.5363 [hep-lat]] [Search INSPIRE].
[10] S. Schaefer, R. Sommer, and F. Virotta [ALPHA Collaboration], Nucl. Phys. B **845**, 93 (2011) [arXiv:1009.5228 [hep-lat]] [Search INSPIRE].
[11] G. I. Egri, Z. Fodor, S. D. Katz, and K. K. Szabó, J. High Energy Phys. **01**, 049 (2006) [arXiv:hep-lat/0510117] [Search INSPIRE].
[12] S. Aoki et al. [JLQCD and TWQCD Collaborations], Phys. Lett. B **665**, 294 (2008) [arXiv:0710.1130 [hep-lat]] [Search INSPIRE].
[13] T. DeGrand and S. Schaefer, arXiv:0712.2914 [hep-lat] [Search INSPIRE].
[14] T.W. Chiu, S. Aoki, S. Hashimoto, T.H. Hsieh, T. Kaneko, H. Matsufuru, J. Noaki, T. Onogi, and N. Yamada [JLQCD and TWQCD Collaborations], PoS LATTICE **2008**, 072 (2008) [arXiv:0810.0085 [hep-lat]] [Search INSPIRE].
[15] T.-W. Chiu, T.-H. Hsieh, and P.-K. Tseng [TWQCD Collaboration], Phys. Lett. B **671**, 135 (2009) [arXiv:0810.3406 [hep-lat]] [Search INSPIRE].
[16] T. H. Hsieh et al. [JLQCD and TWQCD Collaborations], PoS LAT **2009**, 085 (2009).
[17] Y. Aoki et al. [RBC and UKQCD Collaborations], Phys. Rev. D **83**, 074508 (2011) [arXiv:1011.0892 [hep-lat]] [Search INSPIRE].
[18] T.-W. Chiu, T.-H. Hsieh, and Y.-Y. Mao [TWQCD Collaboration], Phys. Lett. B **702**, 131 (2011) [arXiv:1105.4414 [hep-lat]] [Search INSPIRE].
[19] T.-W. Chiu, T.-H. Hsieh, and Y.-Y. Mao [TWQCD Collaboration], PoS LATTICE **2011**, 104 (2011).
[20] D. B. Kaplan, Phys. Lett. B **288**, 342 (1992) [arXiv:hep-lat/9206013] [Search INSPIRE].
[21] Y. Shamir, Nucl. Phys. B **406**, 90 (1993) [arXiv:hep-lat/9303005] [Search INSPIRE].
[22] R. C. Brower, H. Neff, and K. Orginos, Nucl. Phys. Proc. Suppl. **140**, 686 (2005) [arXiv:hep-lat/0409118].
[23] R. C. Brower, H. Neff, and K. Orginos, arXiv:1206.5214 [hep-lat] [Search INSPIRE].
[24] I. Bautista, W. Bietenholz, A. Dromard, U. Gerber, L. Gonglach, C. P. Hofmann, H. Mejía-Díaz, and M. Wagner, Phys. Rev. D **92**, 114510 (2015) [arXiv:1503.06853 [hep-lat]] [Search INSPIRE].
[25] W. Bietenholz, C. Czaban, A. Dromard, U. Gerber, C. P. Hofmann, H. Mejía-Díaz, and M. Wagner, Phys. Rev. D **93**, 114516 (2016) [arXiv:1603.05630 [hep-lat]] [Search INSPIRE].
[26] R. Brower, S. Chandrasekharan, J. W. Negele, and U.-J. Wiese, Phys. Lett. B **560**, 64 (2003) [arXiv:hep-lat/0302005] [Search INSPIRE].
[27] S. Aoki, H. Fukaya, S. Hashimoto, and T. Onogi, Phys. Rev. D **76**, 054508 (2007) [arXiv:0707.0396 [hep-lat]] [Search INSPIRE].
[28] W. Bietenholz, P. de Forcrand, and U. Gerber, J. High Energy Phys. **12**, 070 (2015) [arXiv:1509.06433 [hep-lat]] [Search INSPIRE].
[29] W. Bietenholz, K. Cichy, P. de Forcrand, A. Dromard, and U. Gerber, PoS LATTICE **2016**, 321 (2016) [arXiv:1610.00685 [hep-lat]] [Search INSPIRE].
[30] E. V. Shuryak and J. J. M. Verbaarschot, Phys. Rev. D **52**, 295 (1995) [arXiv:hep-lat/9409020] [Search INSPIRE].
[31] P. de Forcrand, M. García Pérez, J. E. Hetrick, E. Laermann, J. F. Lagae, and I. O. Stamatescu, Nucl. Phys. Proc. Suppl. **73**, 578 (1999) [arXiv:hep-lat/9810033] [Search INSPIRE].

[32] H. Fukaya, S. Aoki, G. Cossu, S. Hashimoto, T. Kaneko, and J. Noaki [JLQCD Collaboration], PoS LATTICE **2014**, 323 (2014) [arXiv:1411.1473 [hep-lat]] [Search INSPIRE].
[33] R. C. Brower et al. [LSD Collaboration], Phys. Rev. D **90**, 014503 (2014) [arXiv:1403.2761 [hep-lat]] [Search INSPIRE].
[34] M. Lüscher, J. High Energy Phys. **08**, 071 (2010); **03**, 092 (2014) [erratum] [arXiv:1006.4518 [hep-lat]] [Search INSPIRE].
[35] M. Lüscher and P. Weisz, J. High Energy Phys. **02**, 051 (2011) [arXiv:1101.0963 [hep-th]] [Search INSPIRE].
[36] C. Bonati and M. D'Elia, Phys. Rev. D **89**, 105005 (2014) [arXiv:1401.2441 [hep-lat]] [Search INSPIRE].
[37] H. Fukaya, S. Aoki, G. Cossu, S. Hashimoto, T. Kaneko, and J. Noaki [JLQCD Collaboration], arXiv:1509.00944 [hep-lat] [Search INSPIRE].
[38] T. Kaneko, S. Aoki, G. Cossu, H. Fukaya, S. Hashimoto, and J. Noaki [JLQCD Collaboration], PoS LATTICE **2013**, 125 (2014) [arXiv:1311.6941 [hep-lat]] [Search INSPIRE].
[39] J. Noaki, S. Aoki, G. Cossu, H. Fukaya, S. Hashimoto, and T. Kaneko [JLQCD Collaboration], PoS LATTICE **2013**, 263 (2014).
[40] G. Cossu, J. Noaki, S. Hashimoto, T. Kaneko, H. Fukaya, P. A. Boyle, and J. Doi, arXiv:1311.0084 [hep-lat] [Search INSPIRE].
[41] The simulation code Iroiro++ can be downloaded from http://suchix.kek.jp/guido_cossu/documents/DoxyGen/html/index.html.
[42] C. Morningstar and M. Peardon, Phys. Rev. D **69**, 054501 (2004) [arXiv:hep-lat/0311018] [Search INSPIRE].
[43] S. Borsányi et al., J. High Energy Phys. **09**, 010 (2012) [arXiv:1203.4469 [hep-lat]] [Search INSPIRE].
[44] S. Hashimoto, S. Aoki, G. Cossu, H. Fukaya, T. Kaneko, J. Noaki, and P. A. Boyle, PoS LATTICE **2013**, 431 (2014).
[45] M. Lüscher, Comput. Phys. Commun. **165**, 199 (2005) [arXiv:hep-lat/0409106] [Search INSPIRE].
[46] B. Fahy, G. Cossu, S. Hashimoto, T. Kaneko, J. Noaki, and M. Tomii [JLQCD Collaboration], PoS LATTICE **2015**, 074 (2016) [arXiv:1512.08599 [hep-lat]] [Search INSPIRE].
[47] J. Gasser and H. Leutwyler, Nucl. Phys. B **250**, 465 (1985).
[48] M. Tomii, G. Cossu, B. Fahy, H. Fukaya, S. Hashimoto, T. Kaneko, and J. Noaki [JLQCD Collaboration], Phys. Rev. D **94**, 054504 (2016) [arXiv:1604.08702 [hep-lat]] [Search INSPIRE].
[49] G. Cossu, H. Fukaya, S. Hashimoto, T. Kaneko, and J.-I. Noaki, Prog. Theor. Exp. Phys. **2016**, 093B06 (2016) [arXiv:1607.01099 [hep-lat]] [Search INSPIRE].
[50] G. Grilli di Cortona, E. Hardy, J. Pardo Vega, and G. Villadoro, J. High Energy Phys. **01**, 034 (2016) [arXiv:1511.02867 [hep-ph]] [Search INSPIRE].